An *in situ* scanning-slit alignment system for Kirkpatrick-Baez optics

Patrick P. Naulleau, Phil Batson, Paul Denham, David Richardson, and James Underwood

Center for X-Ray Optics
Lawrence Berkeley National Laboratory
Berkeley, CA 94720

Abstract: A crucial component to many synchrotron beamlines is the Kirkpatrick-Baez system typically used to condense the synchrotron source to a small illumination spot. The performance of this compound optic often dictates the performance of the entire experimental system. Here we present the design of a Kirkpatrick-Baez system including numerous *in situ* alignment controls and an *in situ* slope-measuring feedback system. Implementation of the system on an extreme ultraviolet undulator beamline is described along with experimental results demonstrating alignment to near diffraction-limited performance.

Keywords: Kirkpatrick-Baez, extreme ultraviolet, synchrotron, metrology, system alignment

1. Introduction

Development of extreme ultraviolet (EUV) lithography[1] as a next-generation microelectronics high-volume fabrication solution has demanded numerous innovations in the area of metrology. Because EUV lithography optical systems are composed of reflective, resonant-stack, multilayer-coated optics,[2] at-wavelength metrology[3] is crucial to the technology development process. Some of the recently developed EUV metrologies include wavefront-measuring interferometry,[4-7] flare-measurement techniques,[8,9] multilayer-mask defect inspection,[10] and high-accuracy reflectometry.[11] The majority of these at-wavelength metrologies utilize synchrotron radiation (both undulator and bend magnet) because of its high brightness and stability characteristics.

A key beam-delivery component for many synchrotron-based metrology stations is the Kirkpatrick-Baez mirror system (K–B).[12] The K–B is often used to focus the synchrotron source, or an intermediate image of the source, onto a spatial-filter system or directly onto a sample. These two-dimensional-focusing systems (Fig. 1) are comprised of two orthogonal glancing-incidence mirrors. For optimal performance each mirror should be elliptical in shape in the focussing direction and have no power in the orthogonal direction. The elliptical shape is most conveniently achieved through bending techniques where nominally flat, width-profiled mirrors are actively bent and held to the desired shape.[13,14]

Near diffraction-limited performance from the K–B is crucial to the performance of several of the EUV metrologies mentioned above. This is particularly true for the EUV phase-shifting point diffraction interferometer (PS/PDI)[6-8] where a spatial-filtering pinhole is required at the focus of the K–B in order to guarantee the coherence and sphericity of the test-optic probe beam. For example, to use the PS/PDI to test a 5×-reduction, 0.3 numerical aperture optic operating at a

wavelength of 13.4 nm one would need a spatial-filtering pinhole with a diameter of approximately 100 nm at the focus of the K–B. Another at-wavelength metrology where diffraction-limited performance is of paramount concern is EUV mask defect inspection. In this metrology system, a reflective EUV mask is scanned underneath a focussed EUV beam and both the specular reflected and scattered energy are monitored. The sensitivity of this system, which ideally should be adequate for sub-50-nm defects, is directly proportional to the probe beam area.[10]

In practice, achieving diffraction-limited performance from these K–B systems requires not only adequate assembly tolerances and degrees of freedom for the alignment[15] but also reliable and quantitative *in situ* feedback. Here we present the design of a K–B system including numerous *in situ* alignment controls and an *in situ* slope-measuring feedback system. Implementation of the system on an EUV undulator beamline is described along with experimental results demonstrating alignment to near diffraction-limited performance. We note that although the motivation and specific implementation described here are based on EUV applications, the methods and results presented are applicable to K–B systems operating in any wavelength range.

The *in situ* K–B mirror slope measurement capability is provided by a scanning-slit mechanism as first described by Hignette et al.[16] This method measures the local slope of the mirrors by illuminating only a small portion of the mirror while monitoring the position of the formed image. For a perfectly shaped system, the image position will be invariant as a function of illuminated position on the mirror; all parts of the mirror direct the light to the same point in the image plane. When the mirrors are misshapen in some way, the image position will vary as a

function of mirror illumination position and the nature of this motion can be used to predict the local slope of the mirror and therefore the required alignment adjustment.

2. EUV interferometry beamline

The K–B used as the basis of the implementation described here is installed at the EUV interferometry beamline at the Advanced Light Source synchrotron radiation facility at Lawrence Berkeley National Laboratory. This beamline[17] (Fig. 2) produces a demagnified image of an undulator source at the image plane of the K–B. In the horizontal direction, the K–B directly demagnifies the source by a factor or 60, whereas in the vertical direction the K–B re-images an intermediate image plane located at the exit slit of the monochromator (Fig. 2). This intermediate image is created by the combination of the M2 mirror and the varied-line-space grating in Fig. 2. Overall the beamline provides a total demagnification of 60 in the vertical direction matching the horizontal direction demagnification; the actual K–B demagnification in the vertical direction is 7.2. With a rectangular entrance numerical aperture of 8×10^{-5} and a demagnification of 60, the beamline has a diffraction-limited peak-to-null resolution of approximately 1.4 μm at a wavelength of 13.4 nm.

A *CODE V*[18] model of the actual K–B system along with the approximate positions of the scanning slits is shown in Fig. 3. The vertically focusing mirror (M5) has an object distance of 5564.71 mm, an image distance of 775.28 mm, and an angle of incidence of 84.5 degrees off normal. The horizontally focusing mirror (M6) has an object distance of 24393.44 mm, an image distance of 406.56 mm, and an angle of incidence of 87 degrees off normal. The mirror separation is 361.95 mm. The vertically- and horizontally-scanning slits are positioned 323 mm in front of M5 and 181 mm in front of M6, respectively. Each mirror is profiled in width such as to ideally bend into elliptical shapes having foci matching the image and object distances. In

each case, the total mirror length between the mirror bend actuators is 200 mm and the mirror width is nominally 30 mm. The active area of the mirrors, as dictated by the 80 μrad input numerical aperture, is 3.85×90.06 mm for M5 and 5.26×74.58 mm for M6.

3. K–B alignment system description

The K–B system has been designed to include a total of 8 alignment actuators: two independent bend actuators on each mirror, tilt (angle of incidence) control on each mirror, and twist control on one end of each mirror. The twist control can be used to guaranty planarity of the two ends of the mirror in the cross-bend direction, and has found to be crucial to diffraction-limited performance.[15] All alignment actuators are picomotor driven with position sensing provided by Linear Variable Differential Transformers (LVDTs). Additionally, the entire K–B can be positioned relative to the rest of the beamline to 6 degrees of freedom using a 6-strut base system. Each mirror is comprised of a width-profiled flat where the profile is designed such that the desired ellipse is obtained when proper bend couples are applied to the ends of the mirror.[13,14]

As described above, separate scanning slits are positioned in front of each mirror. The slits are actuated by DC-servo motors mounted outside the K–B vacuum-chamber housing. The slits can be scanned across the active area of each mirror and can be completely withdrawn from the beam path enabling normal operation of the K–B. Because the mirror actuators described above only effect low-frequency mirror features, the slit size and scan step size can be fairly large. In our case, the slit width was chosen such that 1/10th the mirror active area is illuminated when the slit is in the beam path. Because the slits are installed in planes orthogonal to the beam-propagation direction, the slit sizes are approximately 0.2 mm and 0.5 mm for the horizontally- and vertically-scanning slits respectively.

During normal operation of the K–B, a 45° turning mirror (M7 in Fig. 2) is inserted upstream of the image plane, redirecting the beam downward to the experimental chamber. Monitoring of the image-plane distribution is achieved by way of a fluorescent YAG crystal placed in a plane corresponding to the image plane with the 45° turning mirror removed (Fig. 4). As with the scanning slits, the 45° turning mirror can be retracted from the beam using an externally-coupled DC servo motor.

The local slope of the scanned mirror is measured by monitoring the beam position in the design image plane as a function of scanning-slit position. This is accomplished by imaging the fluorescent YAG crystal onto a CCD with 10-μm pixels using a 20× microscope. The CCD image is sent to a frame grabber where it is digitized and analyzed in a computer. The positional resolution provided by this system has been demonstrated to be better than 0.25 μm. Because the image-position shift throughout a mirror scan simply represents the image blur one would have in normal operation of the K–B, the required minimum position resolution is the target resolution of the final system. For the implementation described here, this resolution is on the order of 1 μm.

4. Scanning-slit sensitivities

Because the K–B includes 8 alignment actuators, it is crucial that the *in situ* metrology system be able to distinguish between various possible alignment errors. Feedback for angle-of-incidence control on each mirror is provided by the absolute position of the image point and does not require the scanning slit mechanism. For the remaining actuated controls, however, the scanning-slit system provides feedback capable of distinguishing between bend and twist errors as well as distinguishing between the two mirrors and the two ends of each mirror. This allows

for the effective use of the twist actuators as well as the independent bend actuators on each end of each mirror.

To determine the sensitivity of this system to various alignment errors, we use a *CODE V* model[15] including the slits to calculate the K–B image as a function of slit position. Each calculated image is then processed to determine the center of mass using the same software used in the experimental setup. The feedback is provided in terms of separate *x* and *y* image shift as a function of slit position.

The first error we consider is defocus error in mirror M5. The mirror is bent such that it focuses 0.5 mm downstream from the design focus. This corresponds to a peak sag error at a distance of 100 mm from mirror center of 0.22 μm. The process of scanning a horizontally-oriented 1-mm diameter slit along the beam in front of M5 in 0.5 mm steps is simulated in *CODE V*. The complete scan effectively covers a mirror length of 89 mm. Figure 5 shows the vertical image shift in microns as a function step number. The displacement is seen to be linear in scan position. No appreciable horizontal image shift was detected. Repeating the same process using the vertical slit positioned in front of M6 resulted in no image shift in either direction.

Next we consider defocus error in mirror M6. The mirror is bent such that the mirror focuses 1 mm downstream from the design focus. The process of scanning a vertically-oriented 0.4 mm diameter slit along the beam in front of M6 in 0.2 mm steps is simulated in *CODE V*. The complete scan effectively covers a mirror length of 65 mm. Figure 6 shows the, again linear, horizontal image shift in microns as a function step number. No appreciable vertical image shift was detected. Repeating the same process using the slit placed in front of M5 resulted in no image shift in either direction.

As described above, the scanning slit diagnosis effectively measures the local slope error of the mirror. Noting that defocus is essentially a quadratic sag error, the slope error is simply linear as seen in the simulations described above.

We summarize the defocus results in Table 1, which shows the scanning-slit sensitivity matrix in terms of total image motion in two orthogonal directions for the two slit scans per mm of defocus. S5 represents the horizontal slit in front of M5 and S6 represents the vertical slit in front of M6, v and h indicate vertical and horizontal direction image shift, respectively.

Because the bendable K–B system described here relies on individual bend couples on each end of each mirror, we also need to consider the effect of asymmetric errors. The first case we consider is downstream bender error on M5. The bend couple error is set to 0.2% positive and negative, respectively, creating a peak sag error of about 1 μm across a mirror length of 200 mm. Figure 7 shows the scanning-slit results for the two cases, respectively. The dashed lines are simply linear reference lines. In this asymmetric bend-error case, non-linearity in the displacement error becomes evident. Figures 5 through 7 also demonstrate that the polarity of the bend error can be surmised from the sign of the image displacement slope.

Next, we consider bend-couple errors of opposite magnitude on the two ends of the mirror. In this case we would expect the slope of the image-position shift to change sign during the scan, which is exactly the behavior demonstrated in Fig. 8 where the bend errors have been set to positive and negative 0.2% on the two ends of the mirror respectively. In this opposite-bend error condition, the image point as a function of position along the mirror retraces its path at some distance along the mirror depending upon the relative amplitudes of the two bend errors.

Because the slope errors for the cases depicted in Figs. 7 and 8 are essentially quadratic, one can surmise the sag errors to be cubic. In terms of classical aberrations, these errors can be seen as similar to a combination of defocus and coma.

Finally we consider mirror twist. The twist coefficient, *T*, is set to 0.5×10^{-6}/mm, where the mirror sag error is defined as *Txy*, with *x* and *y* being the coordinates along the mirror in mm. Along a 200 mm length and a 30 mm width, this represents a peak-to-valley sag error of 3 μm. Table 2 summarizes the results. Although not shown, as was the case for defocus, the displacement is linear in scan position for all entries in Table 2. The effect of twist on either mirror manifests itself in both scans. It is also evident that the effect of twist is almost identical, to within a constant, for the two mirrors. The benefit of this property is that a twist error on one mirror can be corrected by adding twist to the second mirror. The downside, however, is that the scanning-slit metrology cannot unambiguously determine the source of the twist error. We also note that simulations show this canceling property to break down as the compensated twist error gets too large. For the K–B system described here, the maximum compensatable twist error is 28 μm peak-to-valley for M5 and 50 μm peak-to-valley for M6.[15] Observing the sensitivity matrices from Tables 1 and 2, it is evident that the scanning slit method can distinguish between twist and bend errors.

4. Experimental demonstration

As described above, the scanning slit metrology system described here has been incorporated into a K–B system installed on the Advanced Light Source EUV interferometry beamline. This system has facilitated *in-situ* alignment as well as periodic monitoring of K–B performance. Figure 9 shows representative experimental scanning slit data recorded during the initial alignment of the K–B. This data was recorded using the scanning slit in front of the horizontal

focusing mirror and observing horizontal deflection of the image as a function of scanning-slit position. By comparison to the simulation data, it is evident that the mirror suffers from asymmetric and opposite bend error leading to an image blur exceeding 7.5 μm. Repeating the same measurement after bend correction yields the plot in Fig. 10. We see that the asymmetric bend error has been removed and that only a small amount of residual defocus error remains for a total amount of image blur of 2 μm.

After final slit-based alignment, the M7 turning mirror (Fig. 4) was reinserted into the beam and the focused spot characterized at the experimental K–B focal plane using a scanning pinhole method. The beam profile was characterized using a 0.5 μm pinhole positioned in front of a photodiode and recording the photodiode output as a function of pinhole position. Figure 11 shows the reconstructed focal image revealing a 3×7-μm spot. The diffraction-limited spot size based on the known undulator beam parameters and a monochromator exit-slit size of 15 μm is 2×7 μm. Scanning slit optimization based on a surrogate image plane, has indeed enabled the system to achieve near diffraction-limited performance.

Acknowledgements

The authors are greatly indebted to Rene Delano, Gideon Jones, and Drew Kemp for expert fabrication and assembly of the K–B focusing system, and to the entire CXRO staff for enabling this research. This research was supported by the Extreme Ultraviolet Limited Liability Company and the DOE Office of Basic Energy Science.

References

1. R. Stulen and D. Sweeney, "Extreme ultraviolet lithography," IEEE J. Quantum Electron. **35**, 694-699 (1999).
2. J. H Underwood and T. W. Barbee, Jr., "Layered synthetic microstructures as Bragg diffractors for X rays and extreme ultraviolet: theory and predicted performance," Appl. Opt. **20**, 3027-3034 (1981).
3. D. Attwood, G. Sommargren, R. Beguiristain, K. Nguyen, J. Bokor, N. Ceglio, K. Jackson, M. Koike, and J. Underwood, "Undulator radiation for at-wavelength interferometry of optics for extreme-ultraviolet lithography," Appl. Opt. **32**, 7022-7031 (1993).
4. J. E. Bjorkholm, A. A. MacDowell, O. R. Wood II, Z. Tan, B. LaFontaine, and D. M. Tennant, "Phase-measuring interferometry using extreme ultraviolet radiation," J. Vac. Sci. & Technol. B **13**, 2919-2922 (1995).
5. A. K. Ray-Chaudhuri, W. Ng, F. Cerrina, Z. Tan, J. Bjorkholm, D. Tennant, and S. J. Spector, "Alignment of a multilayer-coated imaging system using extreme ultraviolet Foucault and Ronchi interferometric testing," J. Vac. Sci. Technol. B **13**, 3089-3093 (1995).
6. H. Medecki, E. Tejnil, K. A. Goldberg, and J. Bokor, "Phase-shifting point diffraction interferometer," Opt. Lett. **21**, 1526-1528 (1996).
7. K. A. Goldberg, E. Tejnil, S. H. Lee, H. Medecki, D. T. Attwood, K. H. Jackson, J. Bokor, "Characterization of an EUV Schwarzschild objective using phase-shifting point diffraction interferometry," in *Emerging Lithographic Technologies*, David E. Seeger, ed., Proc. SPIE **3048**, 264-270 (1997).
8. P. Naulleau, K. Goldberg, E. Gullikson, and J. Bokor, "At-wavelength, system-level flare characterization of EUV optical systems," Appl. Opt. **39**, 2941-2947 (2000).

9. E. M. Gullikson, "Scattering from normal incidence EUV optics," in *Emerging Lithographic Technologies II*, Yuli Vladimirski, ed., Proc. SPIE **3331**, 72-80, (1998).
10. S. Jeong, L. Johnson, S. Rekawa, C. Walton, S. Prisbrey, E. Tenjil, J. Underwood, and J. Bokor, "Actinic detection of sub-100 nm defects on extreme ultraviolet mask blanks," J. Vac. Sci. Technol. B **17**, 3009-3013 (1999).
11. J. Underwood, and E. Gullikson, "Beamline for measurement and characterization of multilayer optics for EUV lithography," in *Emerging Lithographic Technologies II*, Yuli Vladimirski, ed., Proc. SPIE **3331**, 52-61, (1998).
12. P. Kirkpatrick and A. Baez, "Formation of optical images by x-rays," J. Opt. Soc. Am. **38**, 766-774 (1948).
13. W. Ehrenberg, "X-ray optics: the production of converging beams be total reflection," J. Opt. Soc. Am. **39**, 741-745 (1949).
14. J. Underwood, "Generation of a parallel x-ray beam and its use for testing collimators," Space Science Instrumentation **3**, 259-270 (1977).
15. P. Naulleau, K. Goldberg, P. Batson, S. Jeong, and J. Underwood, "Tolerancing of diffraction-limited Kirkpatrick-Baez synchrotron beamline optics for extreme-ultraviolet metrology," Appl. Opt. **40**, 3703-3709 (2001).
16. O. Hignette, A. Freund, and E. Chinchio, "Incoherent X-ray mirror surface metrology," *in Materials, Manufacturing, and Measurement for Synchrotron Radiation Mirrors*, Proc. SPIE **3152**, 188-199 (1997).
17. D. Attwood, P. Naulleau, K. Goldberg, E. Tejnil, C. Chang, R. Beguiristain, P. Batson, J. Bokor, E. Gullikson, H. Medecki, and J. Underwood, "Tunable coherent radiation in the soft X-ray and extreme ultraviolet spectral regions," IEEE J. Quantum Electron. **35**, 709-720 (1999).

18. CODE V is a registered trademark of Optical Research Associates, 3280 E. Foothill Blvd., Pasadena, CA 91107.

List of figures

Fig. 1. Schematic of typical Kirkpatrick-Baez mirror system (K–B). These two-dimensional-focusing systems are comprised of two orthogonal glancing-incidence mirrors. For optimal performance each mirror should be elliptical in shape in the focusing direction and have no power in the orthogonal direction.

Fig. 2. Schematic of the EUV interferometry beamline at the Advanced Light Source synchrotron radiation facility at Lawrence Berkeley National Laboratory. This beamline produces a demagnified image of the undulator source at the focal plane of the K-B, corresponding to the entrance plane of the experimental station.

Fig. 3. *CODE V* model EUV interferometry beamline Kirkpatrick-Baez (K–B) system. The vertically focussing mirror (M5) has an object distance (d_o) of 5564.71 mm, an image distance (d_i) of 775.28 mm, and an angle of incidence (AOI) of 84.5° from normal. The horizontally focussing mirror (M6) has an object distance of 24393.44 mm, an image distance of 406.56 mm, and an angle of incidence of 87° from normal. The K–B and model include separate scanning slits positioned in front of each mirror. The slits are actuated by DC servo motors and can be scanned across the active area of each mirror or completely withdrawn from the beam path enabling normal operation of the K–B.

Fig. 4. During normal operation of the K–B a 45° turning mirror (M7 in Fig. 2) is inserted to redirect the beam downward to the experimental chamber. Monitoring of the image-plane distribution without disturbing the experimental system is performed in the diagnostics image plane, which corresponds to the experimental image plane with the 45° turning mirror removed. As with the scanning slits, the turning mirror can be retracted from the beam using a DC-servo motor.

Fig. 5. Scanning-slit-sensitivity *CODE V* simulation results. Effect of defocus error on M5. Mirror focus is 0.5 mm beyond the design value. Plot shows the vertical image shift in microns as a function of step number while scanning a horizontally-oriented 1 mm diameter slit vertically along the beam in front of M5 in 0.5 mm steps. The effective scan length across the mirror is 89 mm.

Fig. 6. Scanning-slit-sensitivity *CODE V* simulation results. Effect of defocus error on M6. Mirror focus is 1 mm beyond the design value. Plot shows the horizontal image shift in microns as a function step number while scanning a vertically-oriented 0.4 mm diameter slit horizontally along the beam in front of M6 in 0.2 mm steps. The effective scan length across the mirror is 65 mm.

Fig. 7. Scanning-slit *CODE V* simulation results for downstream-end bend couple error of 0.2% (a) positive (too much bend) and (b) negative. Results show non-linear image displacement.

Fig. 8. Scanning-slit *CODE V* simulation results for opposite magnitude bend-couple errors of 0.2% on two mirror ends.

Fig. 9. Representative experimental scanning-slit data recorded during the initial alignment of the K–B. Data was recorded using the scanning slit in front of the horizontal focusing mirror and observing horizontal deflection of the image as a function of scanning-slit position.

Fig. 10. Scanning-slit data recorded by repeating the same measurement described in Fig. 9 after bend correction. The asymmetric bend error has been removed and only a small amount of residual defocus error remains.

Fig. 11. Characterized focal spot at the experimental K–B focal plane after final slit-based alignment. Characterized performed by using a 0.5 μm pinhole positioned in front of a photodiode and recording the photodiode output as a function of pinhole position. Final focal spot size is 3×7-μm, whereas the diffraction-limited spot size based on the known undulator beam parameters and a monochromator exit-slit size of 15 μm is 2×7 μm.

List of tables

Table 1. *CodeV* modeled slit-scan induced total image motion per mm of defocus. S5 represents the horizontal slit in front of M5 and S6 represents the vertical slit in front of M6, v and h indicate vertical and horizontal direction image shift, respectively. The effective scan length across the mirrors is 89 mm and 65 mm for M5 and M6, respectively.

Table 2. *CodeV* modeled slit-scan induced total image motion per 0.5×10^{-6}/mm of twist. S5 represents the horizontal slit in front of M5 and S6 represents the vertical slit in front of M6, v and h indicate vertical and horizontal direction image shift, respectively. The effective scan length across the mirrors is 89 mm and 65 mm for M5 and M6, respectively.

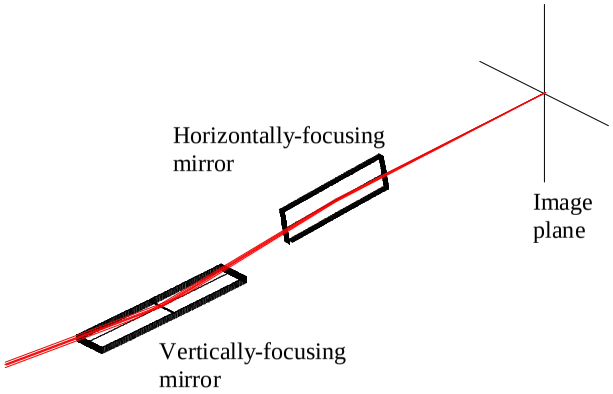

Fig. 1. Schematic of typical Kirkpatrick-Baez mirror system (K–B). These two-dimensional-focusing systems are comprised of two orthogonal glancing-incidence mirrors. For optimal performance each mirror should be elliptical in shape in the focusing direction and have no power in the orthogonal direction.

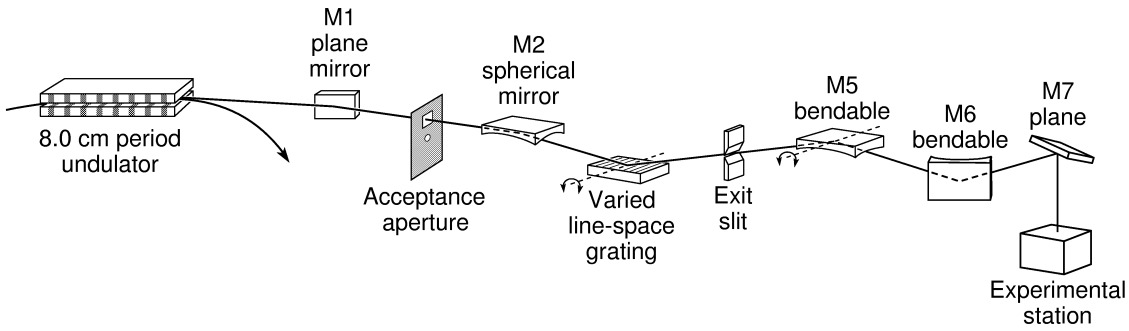

Fig. 2. Schematic of the EUV interferometry beamline at the Advanced Light Source synchrotron radiation facility at Lawrence Berkeley National Laboratory. This beamline produces a demagnified image of the undulator source at the focal plane of the K-B, corresponding to the entrance plane of the experimental station.

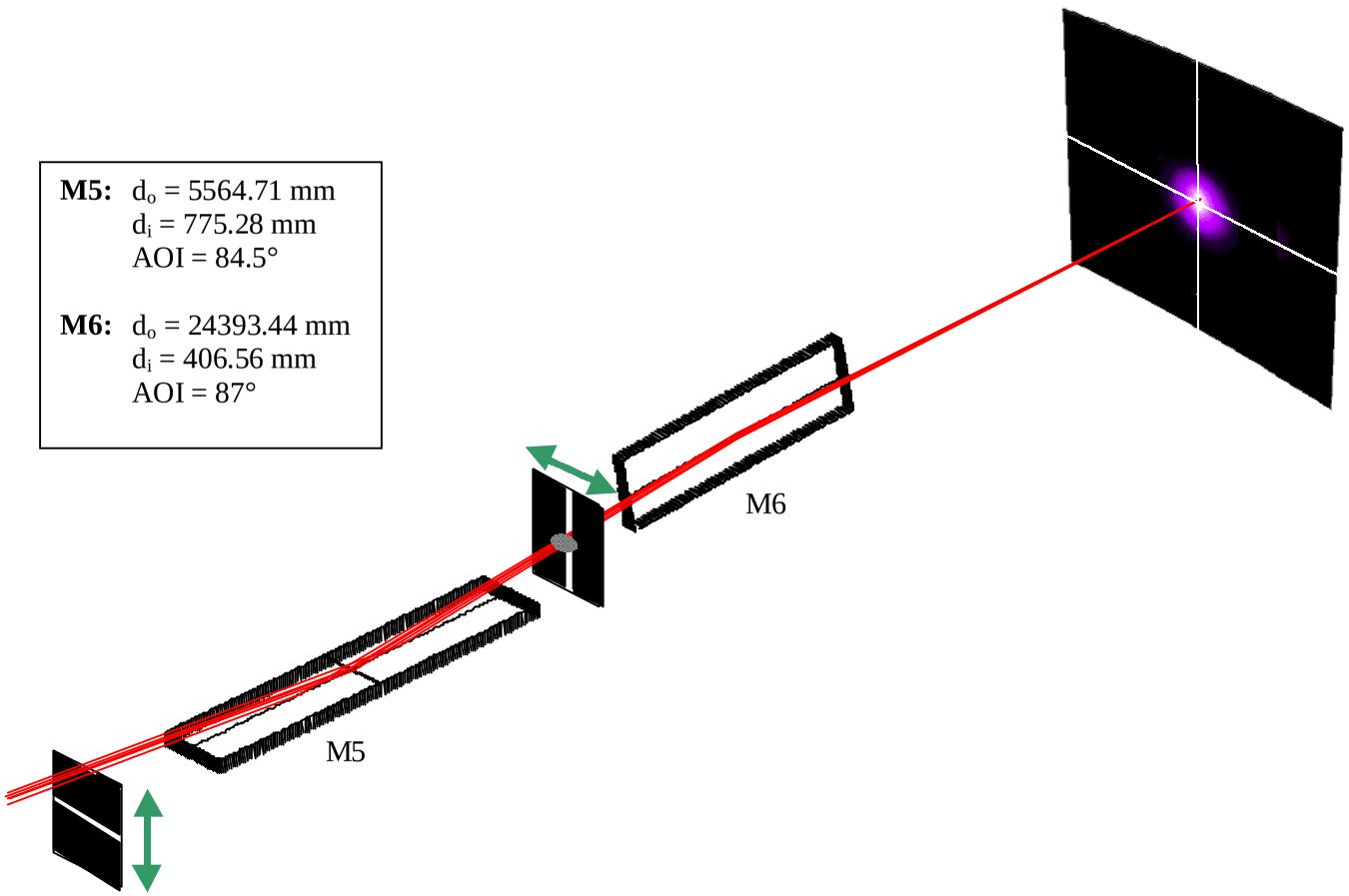

Fig. 3. *CODE V* model EUV interferometry beamline Kirkpatrick-Baez (K–B) system. The vertically focussing mirror (M5) has an object distance (d_o) of 5564.71 mm, an image distance (d_i) of 775.28 mm, and an angle of incidence (AOI) of 84.5° from normal. The horizontally focussing mirror (M6) has an object distance of 24393.44 mm, an image distance of 406.56 mm, and an angle of incidence of 87° from normal. The K–B and model include separate scanning slits positioned in front of each mirror. The slits are actuated by DC servo motors and can be scanned across the active area of each mirror or completely withdrawn from the beam path enabling normal operation of the K–B.

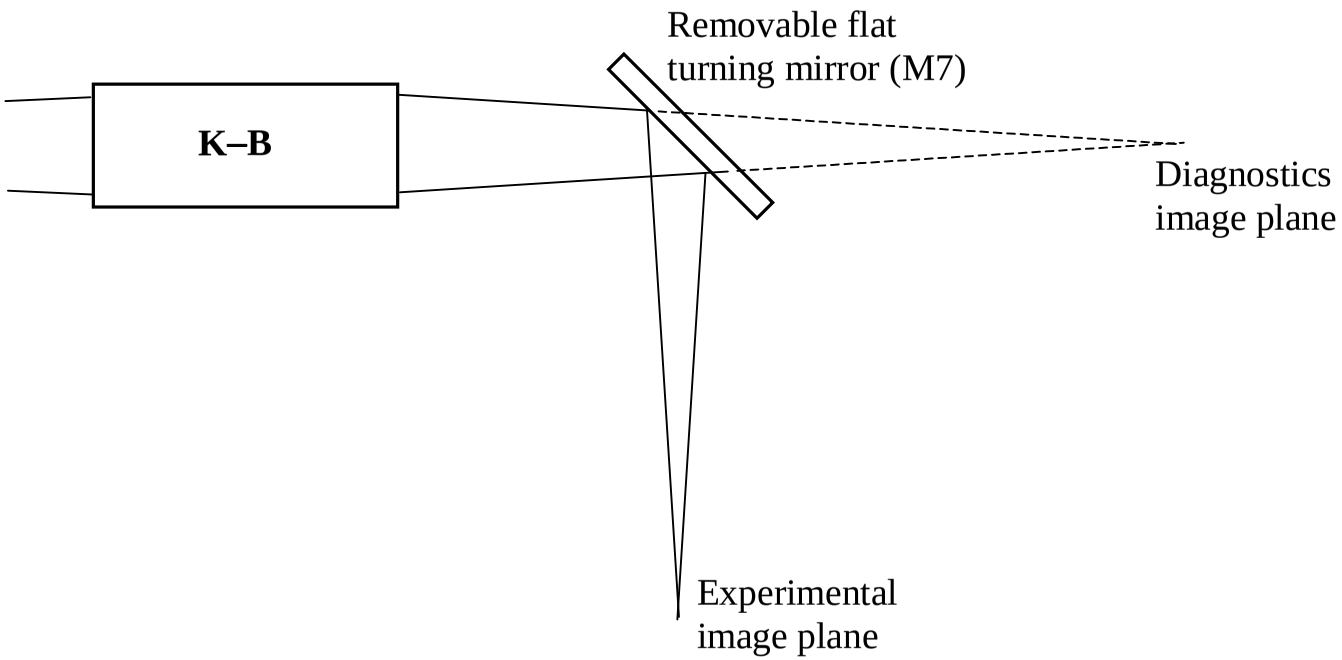

Fig. 4. During normal operation of the K–B a 45° turning mirror (M7 in Fig. 2) is inserted to redirect the beam downward to the experimental chamber. Monitoring of the image-plane distribution without disturbing the experimental system is performed in the diagnostics image plane, which corresponds to the experimental image plane with the 45° turning mirror removed. As with the scanning slits, the turning mirror can be retracted from the beam using a DC-servo motor.

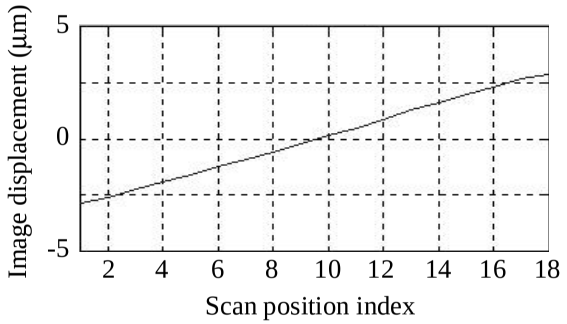

Fig. 5. Scanning-slit-sensitivity *CODE V* simulation results. Effect of defocus error on M5. Mirror focus is 0.5 mm beyond the design value. Plot shows the vertical image shift in microns as a function of step number while scanning a horizontally-oriented 1 mm diameter slit vertically along the beam in front of M5 in 0.5 mm steps. The effective scan length across the mirror is 89 mm.

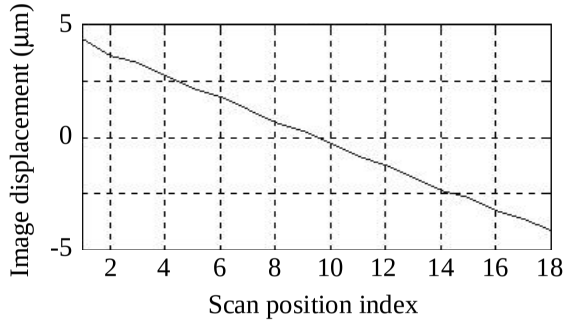

Fig. 6. Scanning-slit-sensitivity *CODE V* simulation results. Effect of defocus error on M6. Mirror focus is 1 mm beyond the design value. Plot shows the horizontal image shift in microns as a function step number while scanning a vertically-oriented 0.4 mm diameter slit horizontally along the beam in front of M6 in 0.2 mm steps. The effective scan length across the mirror is 65 mm.

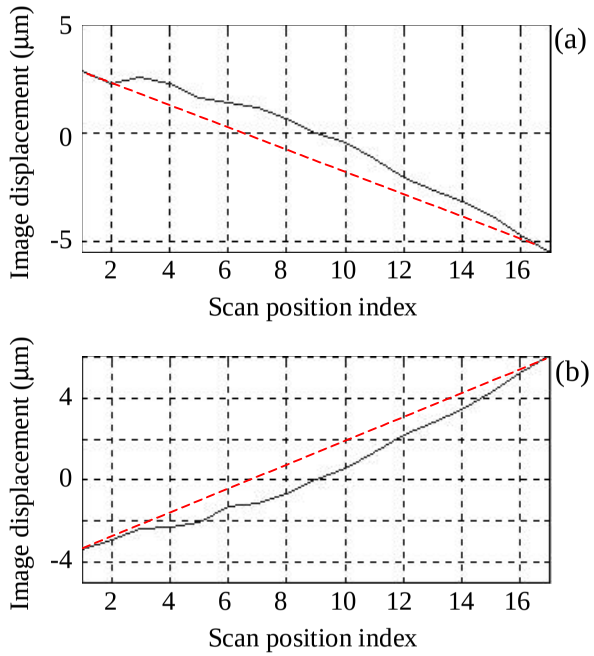

Fig. 7. Scanning-slit *CODE V* simulation results for downstream-end bend couple error of 0.2% (a) positive (too much bend) and (b) negative. Results show non-linear image displacement.

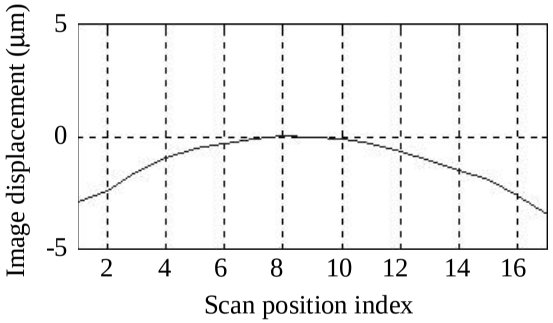

Fig. 8. Scanning-slit *CODE V* simulation results for opposite magnitude bend-couple errors of 0.2% on two mirror ends.

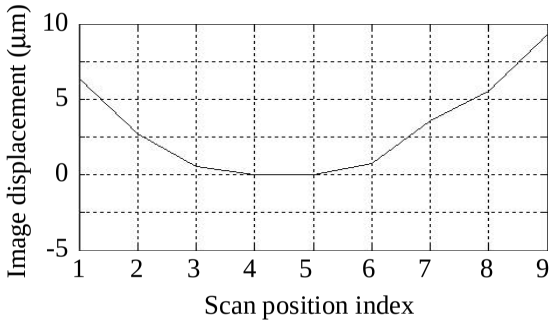

Fig. 9. Representative experimental scanning-slit data recorded during the initial alignment of the K–B. Data was recorded using the scanning slit in front of the horizontal focusing mirror and observing horizontal deflection of the image as a function of scanning-slit position.

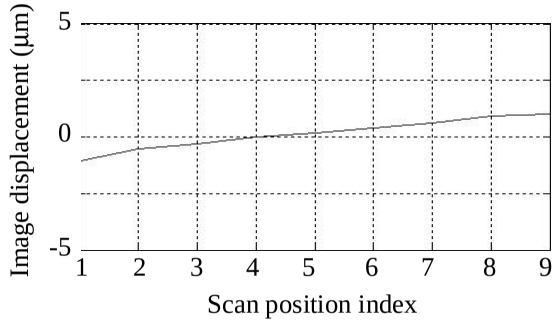

Fig. 10. Scanning-slit data recorded by repeating the same measurement described in Fig. 9 after bend correction. The asymmetric bend error has been removed and only a small amount of residual defocus error remains.

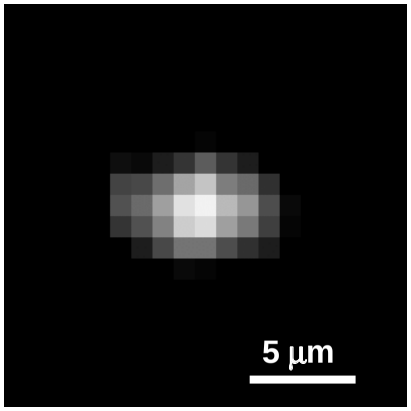

Fig. 11. Characterized focal spot at the experimental K–B focal plane after final slit-based alignment. Characterized performed by using a 0.5 μm pinhole positioned in front of a photodiode and recording the photodiode output as a function of pinhole position. Final focal spot size is 3×7-μm, whereas the diffraction-limited spot size based on the known undulator beam parameters and a monochromator exit-slit size of 15 μm is 2×7 μm.

Scan	Defocus M5	Defocus M6
S5-v	11 μm	0 μm
S5-h	0 μm	0 μm
S6-v	0 μm	0 μm
S6-h	0 μm	-9 μm

Table 1. *CodeV* modeled slit-scan induced total image motion per mm of defocus. S5 represents the horizontal slit in front of M5 and S6 represents the vertical slit in front of M6, v and h indicate vertical and horizontal direction image shift, respectively. The effective scan length across the mirrors is 89 mm and 65 mm for M5 and M6, respectively.

Scan	Twist M5	Twist M6
S5-v	0 μm	0 μm
S5-h	-3.1 μm	2.1 μm
S6-v	2.6 μm	-1.6 μm
S6-h	0 μm	0 μm

Table 2. *CodeV* modeled slit-scan induced total image motion per 0.5×10^{-6}/mm of twist. S5 represents the horizontal slit in front of M5 and S6 represents the vertical slit in front of M6, v and h indicate vertical and horizontal direction image shift, respectively. The effective scan length across the mirrors is 89 mm and 65 mm for M5 and M6, respectively.